Supporting Information

for

Prediction of Specific Biomolecule Adsorption on Silica Surfaces as a Function of pH and Particle Size

by

Fateme S. Emami[†], Valeria Puddu[‡], Rajiv J. Berry[§], Vikas Varshney[§], Siddharth V. Patwardhan[‖], Carole C. Perry[‡*], and Hendrik Heinz[†*]

† Department of Polymer Engineering, University of Akron, Akron, Ohio 44325-0301, USA

‡ Interdisciplinary Biomedical Research Centre, School of Science and Technology, Nottingham Trent University, Clifton Lane, Nottingham NG11 8NS, UK

§ Materials and Manufacturing Directorate, Air Force Research Laboratory, Wright-Patterson Air Force Base, Ohio 45433, USA

‖ Department of Chemical and Process Engineering, University of Strathclyde, 75 Montrose Street, Glasgow G1 1XJ, UK

* Corresponding authors: carole.perry@ntu.ac.uk, hendrik.heinz@uakron.edu

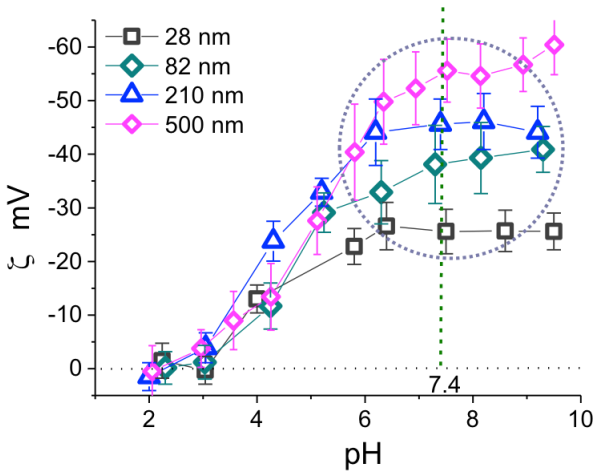

Figure S1. Experimentally measured ζ-potentials of the silica nanoparticles as a function of pH and particle size (from ref. [1]). The total surface ionization increases towards higher pH values and towards larger nanoparticles (highlighted circle). Details of the relationship between surface ionization, fraction of the dissociated cations, and the measured ζ-potential are discussed in ref. [2]. The data are reflected in the chosen silica surface models (Figure 2 and 5a in the main text).

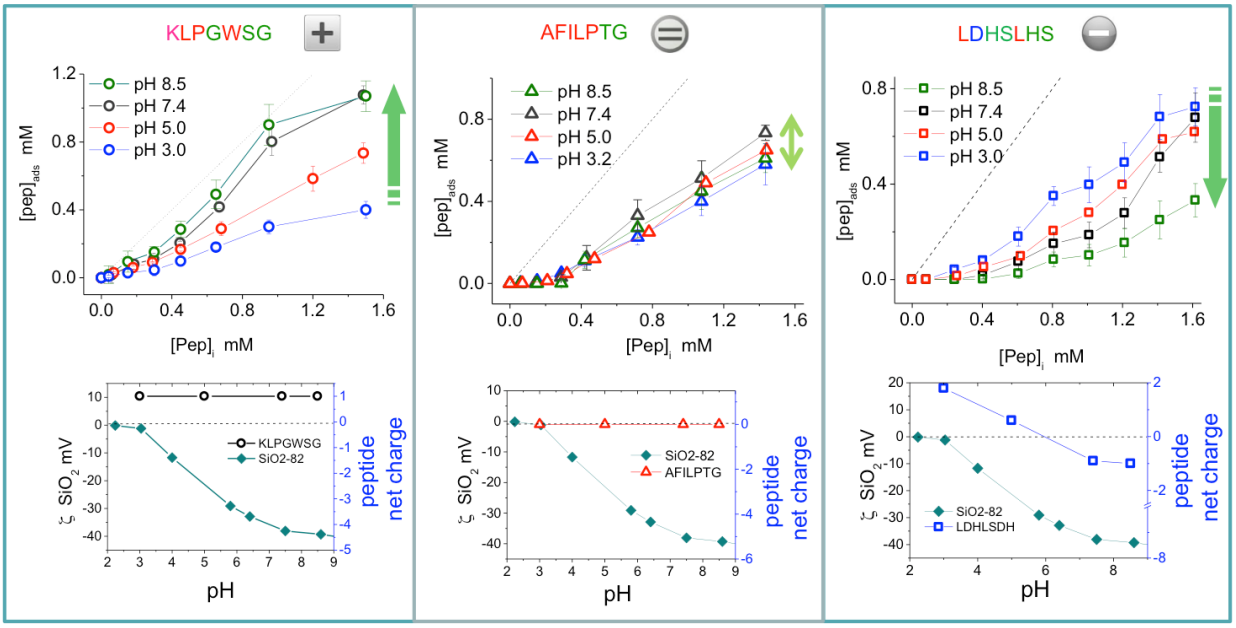

Figure S2. Experimentally measured adsorption isotherms of the peptides on 82 nm silica nanoparticles as a function of pH (from ref. [3]). The upper panels show the adsorption isotherm. The lower panels show the peptide net charge and the ζ potential of neat silica nanoparticles as a function of pH. The adsorbed amount at 1 mM initial peptide concentration was used as a measure of peptide adsorption (Figure 3a in the main text). The colors in the letter sequence of the three peptides indicate hydrophobicity (red), hydrophilicity (green), positive charge of the side chain at pH =7 (pink), and negative charge of the side chain at pH = 7 (blue).

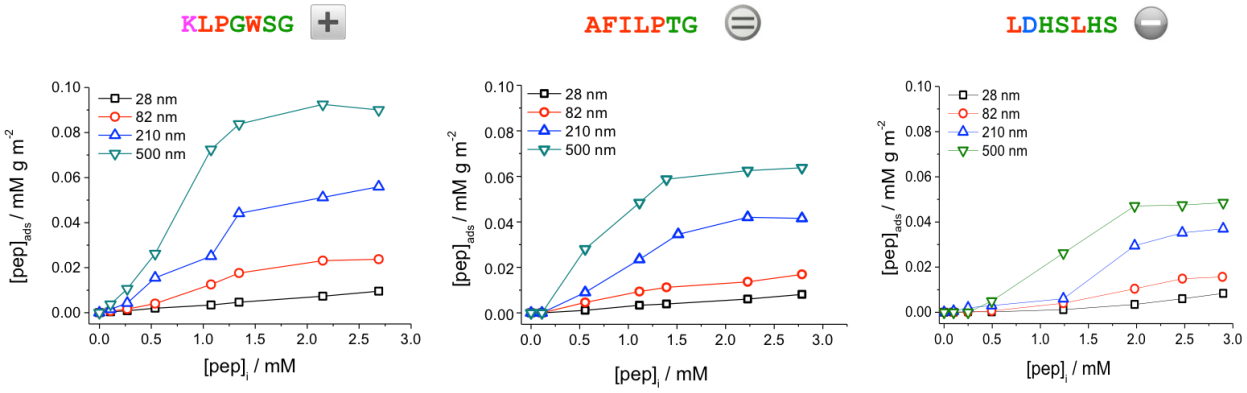

Figure S3. Experimentally measured adsorption isotherms of the peptides on silica nanoparticles at pH = 7.4 as a function of particle size (from ref. [1]). The amount of adsorbed peptide is expressed as an adsorbed concentration of peptide per specific surface area since silica NPs of different size vary in specific surface area. The adsorbed amount for 28, 82, and 210 nm particles at 1 mM initial peptide concentration was used as a measure of peptide adsorption (Figure 5b in the main text).

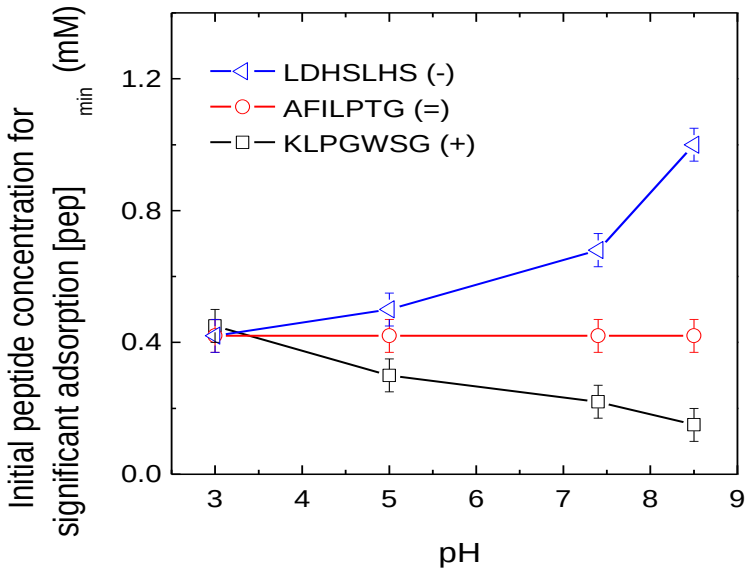

Figure S4. Initial peptide concentration $[pep]_{min}$ required to achieve significant adsorption, defined as ~1 peptide per nm^2, on 82 nm silica nanoparticles as a function of pH according to data from the adsorption isotherms (from data in Figure S2, ref. [3]).

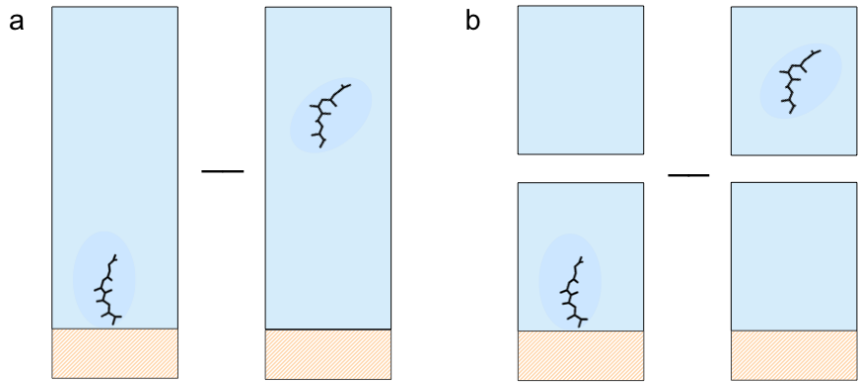

Figure S5. The binding energies of peptides to silica surfaces were calculated as a difference in average energies in the adsorbed versus the desorbed state. (a) Two-box approach. (b) Four-box approach. The two-box approach was preferred because the presence of several ions in solution due to charged peptides and ionized silica surfaces caused long-range interactions that would be misrepresented using additive intermolecular interactions in the four-box approach (see ref. [4]).

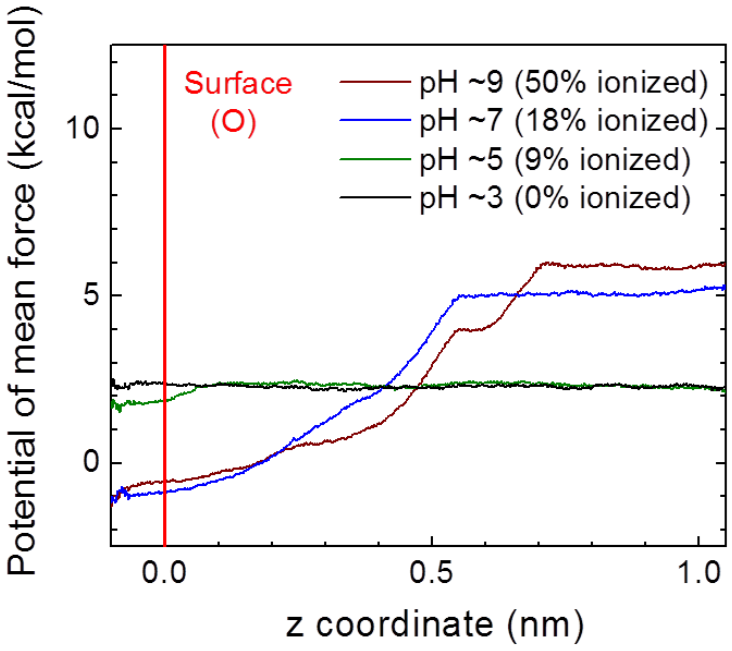

Figure S6. Potential of mean force (PMF) during pull-off of the peptide K^{+}LPGWSG·Cl^{-} from the silica surface using umbrella sampling. The silica surfaces represent 82 nm particles at different pH values. Each curve represents an average over multiple calculations with different start conformations of the peptide on the respective surface. Free energies of adsorption correspond to the difference in PMF at large and small distance (see Table 2 in the main text). The origin of the z coordinate was chosen as the z coordinate of oxygen atoms of silanol and siloxide groups on the silica surface. Peptides penetrate the origin up to 0.1 nm due to cavities in the superficial Si-O rings (see ref. [2]). At yet closer distance, the PMF increases to large positive values due to repulsion.

Table S1. Guide towards surface models for a given silica substrate, as implemented in the silica surface model database in ref. [2]. Essential information includes the area density of SiO(H,Na) groups, the degree of ionization, and the surface topography.

Type of substrate	1. Area density of silanol groups[a]	2. Ionization to (SiO^- M^+)[b]	3. Surface topography
Quartz surfaces, silica nanoparticles >200 nm size, silica at pH > 9	Q^2 and Q^2/Q^3 (9.4 to 4.7 per nm^2)	pH 2: ~0 per nm^2 pH 5: ~0.5 per nm^2 pH 7: ~1.0 per nm^2 pH ≥9: ~1.5 per nm^2	Substrate-specific: smooth, rough, porous[d]
Most silica glasses, porous silica, silica nanoparticles <200 nm size	Q^3 (4.7 per nm^2)	pH 3: ~0 per nm^2 (0%) pH 5: ~0.3 per nm^2 (6%) pH 7: ~0.6 per nm^2 (13%) pH ≥9: ~0.9 per nm^2 (20%)	
Silica surfaces and nanoparticles annealed at 200-1000 °C	Q^3/Q^4 and Q^4 (4.7 to 0 per nm^2)[c]	pH 4: ~0 per nm^2 pH 7: 0-0.6 per nm^2 depending on Q^3 content	

[a] The area density and specific changes from Q^2 to Q^4 surfaces at high temperatures are described in refs. [5, 6]. [b] Physiological conditions with an ionic strength I ~ 0.1-0.3 M of sodium ions are assumed here. Ionization at a given pH for different ionic strength I and other cations must be reevaluated according to data in refs. [7-16]. Note that silica begins to dissolve at pH≥9. [c] Rehydration can lower the Q^4 content in favor of Q^3. [d] Pore parameters include pore shape, diameter, depth, and area density of pores on the surface. Narrow pores likely reduce ionization.

Table S2. Adsorption data for peptide KLPGWSG at different pH values on 82 nm particles from adsorption isotherms (Figure S2), surface coverage, binding constants *K*, and free energies of binding ΔG. The analysis was performed for three different initial peptide concentrations for each pH value. The range of resulting binding constants and free energies is highlighted in bold (see text in the SI).

pH	Initial peptide conc. $[P_0]$ in mM	Conc. of ads. peptide in equ. $[P_A]$ in mM	Conc. of free peptide in equ. $[P]$ in mM	No of adsorbed peptides *d* per nm^2	Surface area covered by peptide $[S\text{-}P]$[a] per nm^2	$\frac{[S-P]}{[S]}$[b]	*K* (eq S4) in M^{-1} and ΔG in kcal/mol (coverage < 1)	*K* (eq S5) in M^{-1} and ΔG in kcal/mol (coverage > 1)
3.0	0.15	0.03	0.12	0.3	0.075-0.75	0.08 … 3.0	**700-25000; -3.9 … -6.0**	8300; -5.3
	0.45	0.09	0.36	0.9	0.22-2.2	0.3 … ~10	**800-25000; -4.0 … -6.0**	**2800; -4.7**
	0.95	0.27	0.68	2.7	0.68-6.8	2.1 … ~100	**3·10^3**-1.5·10^5; **-4.7** … -7.1	**1500; -4.3**
5.0	0.18	0.07	0.11	0.7	0.18-1.8	0.2 … ~10	**2·10^3-9·10^4; -4.5 … -6.8**	9100; -5.4
	0.45	0.16	0.29	1.6	0.4-4.0	0.7 … ~50	**2·10^3**-2·10^5; **-4.5** … -7.2	**3400; -4.8**
	(0.95)	(0.42)	0.53	4.2	1.0-10	~6 … ~1000	**1·10^4**-2·10^6; **-5.5** … -8.6	**1900; -4.5**
7.4	0.18	0.08	0.10	0.8	0.2-2.0	0.25 … ~10	**2.5·10^3-1·10^5; -4.6 … -6.8**	10000; -5.5
	0.45	0.20	0.25	2.0	0.5-5.0	1 … ~50	**4·10^3**-2·10^5; **-4.9** … -7.2	**4000; -4.9**
	0.96	0.80	0.16	8.0	2.0-20	~10 … ~10^4	**6·10^4**-6·10^7; **-6.5** … -10.6	**6200; -5.2**
8.5	0.15	0.1	0.05	1.0	0.25-2.5	0.3 … ~10	**6·10^3-2·10^5; -5.2 … -7.2**	**20000; -5.9**
	0.45	0.27	0.18	2.7	0.68-6.8	2.1 … ~100	**1·10^4**-5·10^5; **-5.5** … -7.8	**5600; -5.1**
	0.95	0.9	0.05	9.0	2.2-22	~10 … ~10^4	**2·10^5**-2·10^8; **-7.2** … -11.3	**20000; -5.9**

[a] The range of values represents the fractional coverage for upright and flat-on orientation of the peptide chains. For example, 0.2-2.0 equals surface coverage with peptides between 20% in upright orientation and 200% (double layer) in flat-on orientation.
[b] For more than 100% coverage, an estimate for temporarily free surface area [S] was made in powers of ten.

Table S3. Adsorption strength of peptides bound to silica surfaces representing nanoparticles with diameter of 210 nm, 82 nm, and 28 nm at pH~7, characterized by the percentage of simulation time in close contact with the surface, i.e., <3 Å vertical distance from the superficial layer of silanol oxygen atoms. Amino acids are ranked in the order of proximity to the surface with the closest first. The particle surfaces were represented by even Q^2/Q^3 and Q^3 surface models with customized ionization (see Figure 5a). Statistical uncertainties in time averages are ±5%.

Peptide	210 nm		82 nm		28 nm (idealized)	
	Time %	Closest residues	Time %	Closest residues	Time %	Closest residues
KLPGWSG (+)	90	N-term, K1 >>> C-term, S6>>P3, W5, L2	75	N-term, K1 >> C-term, S6>>P3, W5, L2	65	N-term, K1>> C term >L2, W5, P3
AFILPTG (=)	70	N-term>> C-term, T6> F2, L4, I3	40	N-term> C-term, T6, F2, L4, I3	50	N-term> C-term, T6, F2, L4, I3, P5
LDHSLHS (−)	45	N-term>> C-term, S7, D2, S4, H3, H6 > L1, L5	40	N-term, C-term > S7, D2, S4, H3, H6, L1, L5	40	N-term, C-term, S7, D2, S4, H3 H6, L1, L5

Table S4. Specific surface area of silica nanoparticles as a function of size according to BET measurements (S) and expectations for spherical particles with a density of ρ = 1.36 g/cm^3 according to equation (S7) (S_G).

Particle size (nm)	S_{BET} (m^2/g)	S_G (m^2/g)	S_{BET}/S_G	Deviation from ideal sphere geometry
210	21	21	1.00	Minor/NA
82	65	54	1.20	Some
28	243	157	1.54	Significant

Movie S1. Desorption of peptides from different silica surfaces by steered molecular dynamics simulation. Nine representative surface-peptide combinations are shown. A vertical force was applied to the peptides so that conformations in equilibrium and upon successive detachment from the surface can be seen, revealing residues of stronger and weaker attraction. The simulation time shown for each system is approximately 4 ns. Differences in nanoparticle size and pH are represented by three different silica models, including Q2/Q3 surfaces with 20% ionization to represent larger nanoparticles at pH = 7 (210 nm), Q3 silica surfaces with 18% ionization to imitate smaller nanoparticles at pH = 7 (82 nm), as well as Q3 silica surfaces with 0% ionization to exemplify smaller nanoparticles at pH = 3 (82 nm). The pull-off path of the three peptides KLPGWSG(+), AFILPTG, and LDHSLHS(-) is shown on each surface. For example, strong interactions of the positively charged N-terminal groups and K side chains with ionized Q2/Q3 surfaces at pH = 7 can be seen, as well as weaker interactions of several residues including W and F with Q3 non-ionized surfaces at pH = 3. Resistance to detachment varies significantly among the individual systems. The movie complements the discussion in section 3 in the main text and is attached as a separate movie file (mpeg-4 format). (Please note that the results reported in the manuscript average over five or six simulations per system, and only one simulation is shown in the movie.)

S1. Computational Details

Sections S1.1 to S1.3 describe the construction of molecular models (Figure 2, Table S1), details of molecular dynamics (MD) simulations, the analysis of peptide binding conformations and energies (Figures 3-6, S5, Tables 2, 3, and S3, Movie S1), and the computation of free energies of peptide adsorption using umbrella sampling and steered MD (Figure S6). Section S1.4 explains the calculation of peptide binding constants to silica nanoparticles and of free energies of adsorption as a function of pH using the data from experimental adsorption isotherms (Table S2).

S1.1. Models. Models of unit cells of α-cristobalite and α-quartz were obtained from published X-ray crystal structures[17-19] to create super cells of the minerals. Models of regular Q^3 and Q^2 surfaces of approximately ~3.5×3.5 nm^2 surface area were obtained by cleavage of the $(10\bar{1})$ plane of α-cristobalite and of the (100) plane of α-quartz, respectively, followed by hydration of dissociated bonds to silanol groups.[2, 20] Models of deprotonated surfaces were obtained by deletion of hydrogen atoms of randomly selected ≡Si–OH groups and addition of sodium counter ions to create sodium siloxide groups ($\equiv SiO^- \cdots Na^+$) to represent the influence of pH and cations (Table S1). Energy minimization of several possible structures with the same amount of ionic groups yet different distributions helped determine the chosen structure of lowest energy, usually the one with largest possible distance between ionic groups. Energy minimization and molecular dynamics simulation, including brief annealing,[21] were carried out to obtain equilibrium coordinates for all newly constructed surfaces.

This procedure to introduce ionic groups can also be applied to amorphous and porous surfaces, though not further pursued in this work. Thereby, the area density of SiO(H, Na) groups and the degree of ionization of SiOH groups are important parameters. Small

uncertainties in the distribution of ionic groups on the surface are negligible compared to choosing the correct number of ionic groups per surface area.

Models of the peptides in appropriate charge states were built using Hyperchem,[22] Materials Studio,[23] and the program psfgen.[24] The peptides were ionized at N termini, C termini, and ionic groups (K, D, H) along with necessary chloride or sodium ions to balance net positive or negative charges depending on pH value. Models of each peptide were built in different conformations corresponding to α-helix, extended, and random coils to set up independent simulations for each surface-peptide combination to verify convergence of equilibrium conformations and energies from the different start structures.

Models of the interfaces of silica, water, and peptide were built by combination of surface slabs, water slabs, and peptide models using the graphical interface of Materials Studio. For simulations with the PCFF-INTERFACE force field, atom types and atomic charges for the peptides and water were assigned by default, and according to the INTERFACE force field[2] for silica. The structures were then ready for simulations using the Discover and LAMMPS programs. For use of the CHARMM-INTERFACE and AMBER-INTERFACE force fields, two further steps were required. First, models of surface slabs, peptides, and water were prepared separately in .pdb and .psf format, and subsequently combined into one .pdb/.psf model using two programs routines provided in the companion paper.[2] The definition of specific CHARMM topology files was not necessary (and not practical) due to the bonded nature and complexity of silica. The structures were then ready for simulations using the NAMD program.

S1.2. Molecular Dynamics Simulation and Analysis of Peptide Binding Conformations and Energies. Conformations and adsorption energies of the peptides on silica surfaces were analyzed as a function of pH and particle size using molecular dynamics simulation of the

peptides adsorbed and detached from the surface (Figures 3, 4, 5, and 6, Movie S1). A two-box approach rather than a faster four-box approach was employed due to long-range Coulomb interactions originating from dissociated surface ions and ionic components of the peptide (Figure S5).[4] Silica models of dimensions ~3.5 × 3.5 nm^2 with ~4.7 silanol groups per nm^2 with 0% (Figure 2a), 9% (Figure 2b), 18% (Figure 2c), and 50% ionization (Figure 2d) were employed (see refs. [2, 20]), along with one peptide molecule and 3200 flexible SPC water molecules. Also, a mixed Q^2/Q^3 silica surface of similar dimensions and 20% ionization was employed (Figure 2e). At least five different initial peptide conformations were chosen on the surface and in solution for each system. Molecular dynamics simulations were carried out for each of these replicas to verify convergence, compute average energies of adsorption, and determine uncertainties. Start conformations for multiple replicas of the same system included α-helix, extended conformations, random coils, and different orientation relative to the surface.

The CHARMM-SILICA (CHARMM-INTERFACE) force field (12-6 LJ potential) was employed along with the program NAMD[24] for all final results since it contains excellent parameters for silica and for the peptides. For initial testing, the PCFF-SILICA (PCFF-INTERFACE) force field (9-6 LJ potential) was also engaged along with the programs Discover and LAMMPS.[25] All atoms were flexible, the time step was 1 fs, the cutoff for van-der-Waals interactions 12 Å, and the accuracy of the summation of long-range Coulomb interactions high at 10^{-6} using Particle Mesh Ewald (PME) and Particle-Particle Particle-Mesh (PPPM) solvers in NAMD and LAMMPS. After initial energy minimization to remove atomic close contacts, every system was annealed for 1 ns in the NVT ensemble at 500 K for conformation relaxation, followed by 1 ns NVT molecular dynamics at 298K, and 6 ns NPT molecular dynamics at 298 K

and 101.3 kPa. Structural and thermodynamic properties were recorded during the last 4 ns of this trajectory.

Analysis of the adsorbed conformations involved visual inspection of all trajectories, average phi-psi maps, and monitoring the average distance of individual residues from the surface. The percentage of time at close distance from the surface was determined for each surface-peptide combination using the average of the five equilibrium trajectories. Binding energies were calculated as the difference in average energy of the peptide in solution and adsorbed on the surface (Table 2).[26] The statistical uncertainty was estimated from differences in average energy among different trajectories of the same system as well as from differences in block averages of the energy over major portions of the trajectory.[27]

It is also noted that the short length of the peptides of 7 amino acids eases conformation sampling although brief annealing was indispensable to obtain equilibrium conformations. Using time-temperature equivalence, 1 ns at 500 K equals approximately 200 ns at 298 K.[28] The necessity for annealing arises because the number of conformational states of the peptide increases exponentially with chain length as C^N whereby C is the number of possible conformation states per amino acid and N the chain length. C was estimated as $C \sim 10$ considering several possible conformational states of phi, psi, and side chain. Therefore, the 7-amino-acid peptides in this study have $\sim 10^7$ rotational states. Conformation sampling of these short peptides is comparatively easy (200 ns correspond to $2 \cdot 10^{11}$ time steps of 1 fs). In contrast, proteins containing 50 amino acids would have $\sim 10^{50}$ rotational states. As a consequence, all individual conformational states of such longer peptides would not be possible to sample using today's most advanced techniques of annealing, replica exchange, and multiple long simulations combined.

S1.3. Computation of Free Energy of Adsorption. Umbrella sampling as well as steered MD simulation techniques were applied to calculate the free energy profile of the KLPGWSG peptide as a function of distance from the surface, starting from close proximity slightly below equilibrium distance to ~1 nm away from the surface using LAMMPS[25] and NAMD[24] programs (Movie S1).

Umbrella sampling was applied using 22 cross-sectional windows above the surface of 0.5 Å thickness each. A harmonic force with a force constant of 4 kcal/(mol·Å^2) was added to the peptide. The Weighted Histogram Analysis Method[29] (WHAM) was applied to calculate the unbiased free energy along the z-coordinate above the surface (Figure S6).

Steered MD was conducted by adding a constant velocity to the peptide to move ~1 nm apart from the surface during the simulation time. A velocity of 2.5×10^{-6} Å/fs and a force constant of 10 kcal/(mol·Å^2) were applied to calculate the added force in each step. All systems were simulated initially for 1 ns to equilibrate, followed by 4 ns NVT simulation at 298 K. Five independent simulations with different initial configuration were completed. The final PMF was calculated using Jarzynski's equation[30] from the accumulated work performed to slowly displace the peptide from the surface. Surface atoms were kept in their initial position by applying steered MD with a velocity equal to zero Å/fs. Uncertainties of computed free energies of adsorption were derived from five independent simulations for each system.

S1.4. Calculation of Peptide Binding Constants and Binding Free Energies from the Experimental Adsorption Isotherms. Adsorption isotherms provide sufficient data to calculate binding constants and free energies of adsorption (Figure S2 and S3). The adsorption-desorption equilibrium can be described at any surface coverage as:

$$SiO_{2-x}(OH, ONa)_{2x} + \text{Peptide (aq)} \rightleftharpoons SiO_{2-x}(OH, ONa)_{2x} - \text{Peptide (bound)} \quad \text{(S1)}$$

$SiO_{2-x}(OH, ONa)_{2x}$ describes the silica nanoparticle with a certain fraction x of hydrated oxygen bridges that constitute silanol groups and sodium siloxide groups on the particle surface. The peptide in aqueous solution (aq) can then reversibly bind to the surface depending on affinity. In a more simplified notation, a free surface S, peptides P in solution, and surface covered with adsorbed peptide S-P can describe this process:

$$S + P \rightleftharpoons S\text{-}P \quad \text{(S2)}$$

Due to the specific interactions of the peptides with the surface (ion pairing, hydrogen bonds, van-der-Waals, folding effects), binding constants vary with concentration even for the same peptide and the same surface. For example, adsorption may be stronger at low concentration of the peptide if the peptide is ionically attracted to the silica surface and much weaker at higher concentration once the surface is covered with peptides and becomes peptide-like rather than silica-like. Figures S2 and S3 confirm that the type of interaction follows no idealized adsorption isotherms, such as the Langmuir isotherm for inert noble gases or Freundlich isotherms.

Therefore, the calculation of binding constants from the adsorption isotherms needs to reflect these dependencies and different approaches can be taken. Following the definition of the equilibrium constant of a process as a product of the mole fractions of products divided by the product of the mole fractions of the educts, and neglecting any potential stoichiometric factors larger than one, two simple approaches appear useful.

The first approach includes details of the solid phase and is assumed to work best for low and medium surface coverage (0% to 100% surface coverage, i.e., below flat-on monolayer coverage[31]):

$$K = \frac{[S-P]}{[S][P]}. \qquad \text{(S3)}$$

Hereby, the ratio of surface area covered by peptide to uncovered surface $[S-P]/[S]$ is determined from the number density d of adsorbed peptides per nm^2 available surface area according to the adsorption isotherms. The value of d was derived using the BET surface area and the molar amount of adsorbed peptide. The approximate spatial demand of the peptides in upright and flat-on conformations was derived from the molecular models, yielding $[S-P]$ and $[S]$. $[P]$ is the concentration of free peptide in solution in equilibrium and directly available from the adsorption isotherms. Equation (S3) may also be the correct solution to determine incremental binding constants at any given surface coverage, taking into consideration the *additional* amount of adsorbed peptide versus the added amount in solution. However, this approach is not taken here; the focus is on low peptide coverage and a cumulative estimate is presented at higher coverage for simplicity.

The second approach neglects details of the solid phase and is assumed to work well for highly covered surfaces when no bare surface area is exposed to solution (>100% surface coverage, i.e., above flat-on monolayer coverage such as partial bilayers, trilayers, etc[31]):

$$K = \frac{1}{[P]} \qquad \text{(S4)}$$

The surface is then fully covered with peptide so that the free energy (chemical potential) of the peptides on the surface equals the free energy (chemical potential) of remaining peptide in solution. The concentration of remaining free peptide in solution $[P]$ is directly available from

the adsorption isotherm. The approach taken in equation (S4) is consistent with expectations in the limit of very high peptide coverage. Then, the concentration in solution will increase to high values consistent with binding constants of $K \leq 1$ that indicate limited further adsorption, i.e., saturation with peptide. However, the neglect of actual specificity of adsorption to the surface renders this approach less suitable to evaluate incremental binding constants as a function of surface coverage, which is not considered for simplicity here.

The computation of free energies of binding from the equilibrium constant *K*, obtained from equation (S3) or from equation (S4) then follows the known relationship:

$$\Delta G = -RT \ln K \qquad \text{(S5)}$$

The calculation of binding constants *K* and free energies of adsorption ΔG from the adsorption isotherms of the peptide S1 (KLPGWSG) as a function of pH is shown in Table S2. Assumptions for the use of equation (S3) include (1) that a concentration of adsorbed peptide $[P_A]$ of 0.1 mM corresponds to *d* ~1.0 peptide per nm^2, derived from the BET specific surface area of the 82 nm nanoparticles of 65 m^2/g, the nanoparticle concentration in solution of 1 mg/ml, and the molar amount of peptide adsorbed, (2) that the area covered on the silica surface per peptide is between 0.25 nm^2 (vertically bound) and 2.5 nm^2 (flat-on), derived from the smallest van-der-Waals cross-sectional area of the peptides in upright orientation and the maximum van-der-Waals area covered in flat-on orientation according to the molecular models in the simulation. In comparison, the cross-sectional area of an all-anti configured alkyl chain is 0.188 nm^2.

Although the analysis of binding data from adsorption isotherms involves some uncertainty as explained above, the following results are obtained (Table S2): (1) The typical adsorption free energy is consistently between -4 and -6 kcal/mol for low initial concentration and low surface

coverage. An increase in binding is observed towards higher pH value. (2) For each pH value, binding free energies diminish towards zero at higher initial peptide concentration (Figure S2). If incremental rather than cumulative binding constants would be considered, binding free energies approach 0 kcal/mol at high initial peptide concentration $[P_0]$ > 2 mM, demonstrated by the plateau of adsorption isotherms (Figure S3). (3) Equation (S4) is in reasonable agreement with equation (S3) at low concentrations and partial surface coverage below 100%. (4) Only the values for lowest initial peptide concentration at each pH value are relevant for comparison with simulation results as they correspond to comparable low surface coverage. The agreement between experiment (Table S2) and simulation (Table 2) is good.

Some uncertainties and further observations are also notable, especially since a previous analysis in such detail may not have been performed. (1) Error bars at low initial peptide concentration are significant. Therefore, free energies of binding from the adsorption isotherm are about ±2 kcal/mol uncertain. (2) Simulation indicates that the proximity of "bound" peptides to the surface differs considerably from one system to another. The distinction of bound peptide versus free peptide $[P]$, as well as of the surface area effectively covered by peptide $[S-P]$ versus available surface $[S]$ depends on these details. Particularly, at low pH values, close contact was only seen about 30% of the time in simulations while close contact was near 100% at high pH values (Table 3). (3) Related to this point, the range of peptide attraction according to the raw adsorption isotherms (Figure S2) and according to simulation results (Table 2) appears to be wider than the binding free energies according to equations (S3) and (S4) represent (Table S2). The fluorimetric assay only detects the peptide concentration in the supernatant solution and loose association of peptide with the surface at low pH values may not be detected. For example, at about 50% surface coverage, the stipulated ratio $[S\text{-}P]/[S]$ is 1.0 if one assumes close

contact, however, it may decrease to nearly 0.1 and [*P*] may slightly increase assuming loose binding (50% surface coverage for 20% of time). As a result, for loosely binding peptides, true binding constants could be one order of magnitude lower with true binding free energies down to ca. -2 kcal/mol, assuming all other data the same. (4) Overall, some uncertainties in the adsorption isotherm, different possible orientation of the peptides on the surface, a likely distribution of attracted peptides in the interfacial region, as well as potential self-assembly of multiple peptides on the surface pose difficulties to exactly evaluate binding constants. At best, estimates of *K* may be reliable within an order of magnitude, corresponding to uncertainties in binding free energies of ±2 kcal/mol, and require about +1 kcal/mol systematic corrections for less surface contact at lower pH. The understanding of such effects, including specific peptide assembly on the surface at higher concentration as well as incremental binding constants as a function of surface coverage, would benefit from further investigation (cumulative binding constants are shown here). The simulation clearly indicates the occurrence of diffuse boundaries between bound and free peptide, and the feasibility of quantitative insight in agreement with observations.

S2. Experimental Details

Silica nanoparticles were synthesized, characterized, and employed for measurements of adsorption isotherms of the peptides as a function of pH at constant nanoparticle size of 82 nm, and as a function of nanoparticle size at constant pH of 7.4 following the procedure described by Puddu et al.[1, 3] Sections S2.1 to S2.3 summarize relevant methods and details from these references (Figure 1a-d, Figures S1 to S3).

S2.1. Synthesis and Characterization of Silica Nanoparticles. Silica nanoparticles were synthesized by a modified Stöber method.[32, 33] Analysis and assays were carried out on the as-synthesized, lyophilized silica powders without annealing and other subsequent treatment. The same batch of silica nanoparticles was used for all measurements pertaining to a given particle size.

Particle size was measured by transmission electron microscopy (TEM) and scanning electron microscopy (SEM) (Figure 1a-d). Scanning electron microscopy (SEM) was run on freeze-dried samples attached to double-sided adhesive tape attached to SEM stubs and coated with carbon (Edwards, sputter coater S150B). The samples were then examined with a JEOL JSM-840A instrument operated at 20 kV. Transmission electron microscopy (TEM) was run on JEOL 2010 operating at 200 kV. Samples were prepared by evaporation of diluted suspensions onto carbon-coated copper grids. The particle size was assessed by averaging the size of a minimum of 50 particles from a SEM or TEM image.

Surface area and porosity were measured by N_2 adsorption-desorption analysis following the BET method on powder samples of approximately 100 mg using a Quantochrome Nova3200e. Samples were degassed at 120 °C overnight prior to analysis. The surface area was determined from a five-point adsorption isotherm in the relative pressure range of 0.05−0.35 at 77.3 K.

Porosity was evaluated from the desorption branch using the Barrett−Joyner−Halenda (BJH) method. Mesoporosity was identified for the 28 nm and 82 nm particles, whereas microporosity (<2 nm) associable with the individual particles could not be identified.

Thermogravimetric analysis (TGA) was run on 3−7 mg of material using a TGA/SDTA 851 Mettler Toledo, heating from 30 to 800 °C at a 10 °C/min heating rate under a dry N_2 flow. The silanol density per surface area *a* (silanol number) was calculated from the weight loss in the region of 150−800 °C using the following formula:[34]

$$a / nm^2 = \frac{2\left[wt(T_l) - wt(T_h)\right]}{M_{H_2O}} \frac{N_A}{S_{BET}}. \quad \text{(S6)}$$

Thereby, $wt(T_l)$ was the weight at 150 °C, $wt(T_h)$ the weight at 800 °C, M_{H_2O} the molecular weight of water, N_A the Avogadro constant, and S_{BET} the BET specific surface area normalized to the weight $wt(T_l)$. The factor two arises from the condensation of two superficial SiOH groups into one Si-O-Si bridge under elimination of one water molecule. The silanol number determined (Figure 5) may be slightly underestimated because some internal and isolated silanol groups require temperatures up to 1100 °C to condense.[5, 6] The results for small nanoparticles (*a* = 4.5 nm^{-2}), however, closely match literature expectations for amorphous nanoparticles (*a* = 4.6-4.7 nm^{-2}). Therefore, underestimates are likely less than 5% and would hardly affect comparisons to model predictions.

ζ-Potential titrations were carried on 1 mg/mL silica suspensions in 10^{-3} M HCl with 10^{-3} M KOH. The ζ-potentials were recorded on 1 mL of suspension in a capillary cell using a Malvern Zetasizer nano-S (Figure S1).

X-ray photoelectron spectroscopy (XPS) was performed on acid (HCl)-washed samples using a Surface Science M-probe XPS spectrometer with a Al Kα source (1486.6 eV) operated at a base pressure of $3 \cdot 10^{-7}$ Pa using step sizes of 0.01 eV for high-resolution XPS analysis and 1 eV for a general XPS survey. XPS of native and peptide-modified nanoparticles in the freeze-dried state confirmed the adsorption of organic material.

The surface chemistry was further analyzed by infrared spectroscopy using a Nicolet Magna IR 750 spectrometer, recording spectra at 4 cm^{-1} resolution and averaging 256 scans, which showed the absence of organic material on the neat silica nanoparticles and peptide adsorption after binding measurements.

S2.2. Synthesis of Peptides. The three peptides identified by phage display (Table 1) were synthesized in-house by microwave-assisted solid phase synthesis (Discover SPS microwave peptide synthesizer) as previously described.[35] Peptides were characterized by matrix-assisted laser desorption ionization (MALDI) mass spectroscopy, and their purity (>85%) was assessed by high-performance liquid chromatography−mass spectroscopy (HPLC−MS).[1]

S2.3. Measurement of Peptide Adsorption Isotherms. The adsorption of peptides was detected using fluorimetric assay. For this purpose, suspensions of silica (1 mg/ml) in phosphate-buffered saline (PBS) containing 100 mM phosphate and 150 mM NaCl were sonicated for 1 h, and suitable amounts of peptide were added in order to achieve the desired initial peptide concentration. The mixtures were shaken vigorously. The suspension was left to equilibrate for 1 h at room temperature and then centrifuged (13 000 rpm for 5 min). The amount of peptide left in solution was quantified by fluorimetric spectroscopy. In a typical assay, 20 μl of fluorescamine (5 mg/ml in acetone) was added to a 180 μl aliquot of the supernatant in a 96-well plate, and the fluorescence intensity was measured using a Tecan Spectrafluor XFLUOR4 plate

reader equipped with a 360 nm excitation filter and a 465 nm absorption filter. The concentration of each peptide was calculated using a peptide-specific calibration curve, and the amount of peptide adsorbed was calculated by difference from the initial peptide concentration. All assays were repeated three times in order to guarantee their repeatability.

The relevant adsorption isotherms for this study are shown in Figure S2 as a function of pH,[3] and in Figure S3 as a function of particle size.[1]

S3. Additional Characteristics of Specific Peptide Binding as a Function of pH

In section S3.1, the minimum initial peptide concentration to achieve significant peptide adsorption and its relation to computed binding energies is discussed. Section S3.2 briefly explains an expected decrease in peptide attraction to silica nanoparticles annealed at high temperature.

S3.1. Threshold Concentration of Peptide for Significant Adsorption. An additional adsorption characteristic is the required threshold concentration of peptide to achieve significant adsorption (Figure S4). Such a threshold concentration, here leading to more than 1 adsorbed peptide per nm^2 according to the adsorption isotherm, characterizes the attraction of peptides to silica particles in the dilute regime. For silica particles of 82 nm size with a specific surface area of ~65 m^2/g and a concentration of 1 mg/ml used in the measurement of peptide adsorption as a function of peptide concentration, a surface coverage of 1 peptide per nm^2 is equivalent to ~0.1 mM of adsorbed peptide.[3] The minimum initial peptide concentration to achieve such significant adsorption is called $[pep]_{min}$, and the lower its value the stronger the peptide is attracted to the surface (Figure S4).

The trend of $[pep]_{min}$ as a function of pH (Figure S4) is inversely proportional to the adsorbed amount of peptide and to the computed attraction to the surface (Figure 2). The positively charged peptide KLPGWSG(+) shows a decrease in $[pep]_{min}$ at higher pH due to stronger ion pairing with negative surface charges. The overall neutral peptide AFILPTG (=) shows no visible dependence of $[pep]_{min}$ as a function of pH. The negatively charged peptide LDHSLHS(-) with pH-dependent adaptation of its own charge shows an increase in $[pep]_{min}$ toward higher pH, i.e., decreased adsorption, as its negative charge and electrostatic repulsion from the negatively charged silica surface increase.

It is noted that in an earlier study a lower surface coverage of ~0.1 peptides per nm^2 was associated with the threshold concentration $[pep]_{min}$,[7] related to larger 12mer peptides and to an underestimate of the density of silica nanoparticles that was revised in this work (~2.0 g/cm^2). The correlation with adsorption energies remains the same in both cases.

S3.2. Thermally Annealed Surfaces. Previous experimental work has also shown the effect of heat treatment of the 82 nm nanoparticles.[3] Upon annealing for 1 h at 600 °C, the silica surfaces attract significantly less peptide. Annealing at this temperature causes partial condensation from Q^3 surface chemistry to a mixed Q^3/Q^4 surface chemistry with significant loss of silanol groups and of ionization per surface area (see Table S1 for typical surface chemistry).[2, 5, 6] As a consequence, attraction of peptides and of water is reduced, including contact angles up to 42°. The trends in diminished binding can be reproduced using simulations with appropriate Q^3/Q^4 surface models given in ref. [2]; more details would exceed the scope of this work.

S4. Further Discussion of Peptide Adsorption on Silica Nanoparticles of 28 nm Size

While particles of 82 nm, 210 nm, and larger size are near-spherical and exhibit well-defined surfaces, particles of 28 nm size are poorly defined (Figure 1). A comparison of the experimentally measured specific surface area S_{BET} from BET measurements with the geometric expectation value of the specific surface area S_G for an ideal sphere provides additional understanding (Table S4). For an ideal sphere, the specific surface area S_G is inversely proportional to the density r and to the radius *r*:

$$S_G = 3/(r \times r). \quad \text{(S7)}$$

This relationship follows from the definition of the specific surface area as the surface area *A* per mass *m*:

$$S_G = A/m = A/(r \times V) = 4\pi r^2/(r \times (4/3)\pi r^3) = 3/(r \times r). \quad \text{(S8)}$$

Assumption of a density of r = 1.36 g/cm^3 for the well-defined, nonporous 210 nm nanoparticles matches the geometric specific surface area to the BET specific area (Table S4). For smaller particle size *r*, however, the measured specific surface area in experiment S_{BET} (Figure 5a) does not correspond to the expected proportionality $S_G \sim 1/r$ (Table S4) and increases more than the geometric expectation value S_G. The gap exceeds 50% for the 28 nm nanoparticles, which can also not be explained by a decrease in particle density (must remain higher than water). The excess BET area therefore suggests porosity and irregularity for the 28

nm nanoparticles. BJH porosity measurements identified no microporosity (<2 nm) for 28 nm particles, however, and thus the presence of irregular inner void spaces rather than ordered pores is suggested. Poor definition, plasticity, and incomplete dissociation of organic precursor were also reported in other studies of silica particles smaller than ~50 nm.[36]

Therefore, it appears reasonable to assume an irregular aggregate interior of the 28 nm nanoparticles with void spaces that connect to the outside. Accordingly, small nitrogen molecules in BET tests could penetrate and explain the high BET area while comparatively large peptide molecules have no entry. This hypothesis explains the disproportionately weak adsorption of peptides observed in experiment (Figure 5b, Figure S3). Peptide adsorption might also be reduced by the presence of residual hydrophobic organic groups on the exterior and interior surfaces of the 28 nm particles.

The use of idealized even surfaces for simplicity in this work (Figure 2 and 5) highlights the impact of morphology on adsorption strength of the peptides and clearly shows that changes in topology are non-negligible. The construction of realistic models of irregular, amorphous silica nanoparticles of small size can be further explored in follow-on efforts, and the reproduction of adsorption isotherms may be one path to validation. The investigation of ligand binding to porous and partially hydrolyzed silica structures could also provide essential insight into the binding mechanism under confinement, help explain mechanisms of mineralization, and capture of specific molecules (e.g. CO_2).

Supporting References

1. Puddu, V.; Perry, C. C. *Langmuir* **2014**, 30, 227-233.
2. Emami, F. S.; Puddu, V.; Berry, R. J.; Varshney, V.; Patwardhan, S. V.; Perry, C. C.; Heinz, H. *Chem. Mater.* **2014**, 26, 2647-2658.
3. Puddu, V.; Perry, C. C. *ACS Nano* **2012**, 6, 6356-6363.
4. Heinz, H. *J. Comput. Chem.* **2010**, 31, 1564-1568.
5. Zhuravlev, L. T. *Colloids Surf., A* **1993**, 74, 71-90.
6. Zhuravlev, L. T. *Colloids Surf., A* **2000**, 173, 1-38.
7. Patwardhan, S. V.; Emami, F. S.; Berry, R. J.; Jones, S. E.; Naik, R. R.; Deschaume, O.; Heinz, H.; Perry, C. C. *J. Am. Chem. Soc.* **2012**, 134, 6244-6256.
8. Bolt, G. H. *J. Phys. Chem.* **1957**, 61, 1166-1169.
9. Tadros, T. F.; Lyklema, J. *J. Electroanal. Chem. Interfacial Electrochem.* **1968**, 17, 267-275.
10. Abendroth, R. P. *J. Colloid Interface Sci.* **1970**, 34, 591-596.
11. Yates, D. E.; Healy, T. W. *J. Colloid Interface Sci.* **1976**, 55, 9-19.
12. Milonjić, S. K. *Colloids Surf.* **1987**, 23, 301-312.
13. Zerrouk, R.; Foissy, A.; Mercier, R.; Chevallier, Y.; Morawski, J.-C. *J. Colloid Interface Sci.* **1990**, 139, 20-29.
14. House, W. A.; Orr, D. R. *J. Chem. Soc., Faraday Trans.* **1992**, 88, 233-241.
15. Sonnefeld, J. *J. Colloid Interface Sci.* **1996**, 183, 597-599.
16. Méndez, A.; Bosch, E.; Rosés, M.; Neue, U. D. *J. Chromatogr. A* **2003**, 986, 33-44.
17. Dera, P.; Lazarz, J. D.; Prakapenka, V. B.; Barkley, M.; Downs, R. T. *Phys. Chem. Miner.* **2011**, 38, 517-529.

18. Kihara, K. *Eur. J. Mineral.* **1990**, 2, 63-77.

19. *Silica: Physical Behavior, Geochemistry, and Materials Applications*. Heaney, P. J., Prewitt, C. T., Gibbs, G. V., eds., In: Reviews in Mineralogy, Vol. 29; Mineralogical Society of America: New Jersey, USA, 1994.

20. Heinz, H.; Lin, T.-J.; Mishra, R. K.; Emami, F. S. *Langmuir* **2013**, 29, 1754-1765.

21. Fu, Y. T.; Heinz, H. *Chem. Mater.* **2010**, 22, 1595-1605.

22. *HyperChem 7.5*, Hypercube Inc.: Gainesville, FL, 2006.

23. *Material Studio 4.1 and Discover Program*, Accelrys Inc: San Diego, CA, 2006.

24. Phillips, J. C.; Braun, R.; Wang, W.; Gumbart, J.; Tajkhorshid, E.; Villa, E.; Chipot, C.; Skeel, R. D.; Kale, L.; Schulten, K. *J. Comput. Chem.* **2005**, 26, 1781-1802.

25. Plimpton, S. *J. Comput. Phys.* **1995**, 117, 1-19.

26. Andersen, H. C. *J. Chem. Phys.* **1980**, 72, 2384-2393.

27. Feng, J.; Pandey, R. B.; Berry, R. J.; Farmer, B. L.; Naik, R. R.; Heinz, H. *Soft Matter* **2011**, 7, 2113-2120.

28. Jha, K. C.; Liu, H.; Bockstaller, M. R.; Heinz, H. *J. Phys. Chem. C* **2013**, 117, 25969-25981.

29. Kumar, S.; Bouzida, D.; Swendsen, R. H.; Kollman, P. A.; Rosenberg, J. M. *J. Comput. Chem.* **1992**, 13, 1011-1021.

30. Jarzynski, C. *Phys. Rev. Lett.* **1996**, 78, 2690-2693.

31. Heinz, H.; Vaia, R. A.; Krishnamoorti, R.; Farmer, B. L. *Chem. Mater.* **2007**, 19, 59-68.

32. Roach, P. F., D.; Perry, C. C. *J. Am. Chem. Soc.* **2006**, 128, 3939-3945.

33. Stober, W.; Fink, A.; Bohn, E. *J. Colloid Interface Sci.* **1968**, 26, 62-69.

34. Kim, J. M.; Chang, S. M.; Kong, S. M.; Kim, K. S.; Kim, J.; Kim, W. S. *Ceram. Int.* **2009**, 35, 1015-1019.

35. Naik, R. R.; Brott, L. L.; Clarson, S. J.; Stone, M. O. *J. Nanosci. Nanotechnol.* **2002**, 2, 95-100.

36. Costa, C. A. R.; Leite, C. A. P.; Galembeck, F. *J. Phys. Chem. B* **2003**, 107, 4747-4755.